Theor Chem Acc (2012) 131:1130
DOI 10.1007/s00214-012-1130-1

REGULAR ARTICLE

New insights into oxidation properties and band structure of fluorescein dyes from ab initio calculations

Francesco Buonocore · Andrea di Matteo

Received: 16 June 2011 / Accepted: 6 August 2011 / Published online: 14 February 2012

Abstract During recent years, several publications have investigated the electrical bistability of spin cast films of halogenated fluorescein dyes. In the present contribution, we simulate the excited states of single fluorescein dyes with time-dependent density functional theory (TD-DFT) and we analyzed the band structure of the corresponding molecular crystals with DFT. More precisely, the molecules examined are fluorescein, erythrosine B, and rose bengal. We consider the molecular crystals of fluorescein in salt and lactone forms as well as erythrosine B. Rose bengal showed high quantum yield of the triplet state and high electronic affinity. Therefore, the rose bengal has very strong oxidation properties and it is able to form electrically bistable thin oxide layer. The poor crystal order and small bandwidths of fluorescein in salt form and erythrosine B indicated high resistivity for both crystals.

Keywords Fluoresceins · Electrical bistability · DFT · TD-DFT

Dedicated to Professor Vincenzo Barone and published as part of the special collection of articles celebrating his 60th birthday.

F. Buonocore · A. d. Matteo (✉)
STMicroelectronics Srl, via Remo de Feo 1,
Arzano, Naples, Italy
e-mail: andrea.di-matteo@st.com

F. Buonocore
e-mail: francesco.buonocore@st.com

F. Buonocore · A. d. Matteo
IMAST Scarl P.le E. Fermi, 1 Localita' Granatello,
80055 Portici, Naples, Italy

1 Introduction

In recent years, several publications [1–6] have been reported investigating the electrical bistability of spin cast films of halogenated fluorescein dyes (FDs). Indeed, the switch from a low conduction state to a high conduction state has been reported in the current–voltage electrical characteristic when a voltage threshold $+|V_{th}|$ is reached. The switch is reversible in the sense that the electrical characteristic commutates back to the original state of conduction for a voltage $-|V_{th}|$. In the experiments, the organic film is spin cast on ITO or ZnO substrate and aluminum top electrode is evaporated. In particular, an ON/OFF ratio as high as 350,000 has been reported for electrical current of the rose bengal (RB) films, attributed to the very low OFF current, also compared to the OFF current of the fluorescein films indeed with a quite low ON/OFF ratio. Those promising developments suggest it might be possible to demonstrate and to build up high-density memory devices based on electrically bistable fluorescein films.

Until present days, several mechanisms have been proposed to explain and understand the electrical bistability of FDs, and in our opinion, the debate is still open.

The proposed mechanisms can be resumed as follows: (a) the electrical external field (bias), induces a redox equilibrium between two states: the two redox states inside bandgap have different alignments with respect to the electrodes work function and the electrical response is due to different injection or extraction probability of hole/electron observed for the two states; (b) the electrical external field (bias), induces a charge transfer of electrons from one of the electrodes to the FD molecules increasing the conjugation, by increasing the coplanarity between xanthene and phenyl ring moieties (conformational change); (c) the organic material acts as an insulating layer

in which a conductive path can be generated by one-dimensional "filament" connecting some conductive elements by quantum tunneling: the conductive elements can be either metal ions diffused from electrodes or oxygen vacancies; (d) the mechanism of switching is an interface effect between organic layer and top electrode (aluminum or other metal) where the resistive switching ratio depends on the nature of the oxide and layer thickness.

In the models (a) and (b), the resistive switching is an *intrinsic* effect due to the properties of the organic material, while for mechanisms (c) and (d), the resistive switching is an *extrinsic* effect due either to the electro-formed filament or to the oxide at the metal electrode-organic layer interface.

When the resistive switch was evidenced the first time [1], it was attributed to the change of conjugation (mechanism b). Moreover, Fazzi et al. [7] made accurate calculations and estimated the level alignment at the organic/inorganic interfaces with ITO and aluminum of the neutral and charged molecules (mechanism a). Recently, some papers [5, 6] suggested that the mechanism of switching is completely extrinsic. Jakobsson [5] evidenced the existence of switchable hot spots due to the existence of highly conducting filaments (mechanism c). Kärthauser [6] supported the hypothesis of a conduction switch generated by the thin aluminum oxide layer at the interface (mechanism d). Indeed, it has been observed that binary oxide layers can be electrically bistable [8–17]. Moreover, as it will be discussed later, the RB has an efficient electron transfer with oxygen to give the superoxide anion, O_2^{*-}. It is worthy underline that the four proposed mechanisms (a), (b), (c), and (d) originating the electrical bistability of FD film/electrodes system are not only alternatives to each other, but they could also coexist in the inorganic–organic structure.

The models (a) and (b) are very simple and they can be used to explain the electrical response of a single molecule addressed by two electrodes. However, we stress that the behavior of molecular systems is correlated with both the bulk and hetero junctions interface effects, which are completely neglected in the single molecule models. Therefore, the investigation of the molecular crystal details and the chemical processes at the organic/electrode interface are necessary.

In this paper, more insights into the role of the FD molecules in the generation of the oxide at the interface are given, which is probably responsible for the resistive switching in the extrinsic mechanism (d). Indeed, FDs possess excited triplet states of appropriate energy to be efficient sensitizers of singlet oxygen that could oxidize electrodes at a faster rate than the reaction involving triplet oxygen. FDs exhibited high adsorption coefficient in the green area of the visible spectrum (480–550 nm) and high quantum yield of the triplet state with long triplet states lifetimes. Therefore, xanthene dyes possess the required properties to be photosensitizer of singlet oxygen with high yields. The mechanism of photosensitization of singlet oxygen is described later. Increasing the atomic mass of halogen substituents increases also the yield of intersystem crossing to the triplet state of the dye; for this reason, RB is a more efficient photosensitizer. Moreover, we observe that there is a lack of papers appeared in literature concerning the electronic structure of FD crystals and the correlation with electrical conduction properties. Our investigations originated from the well-known aggregation phenomena in xanthene dyes. The charge transport properties in organic crystals depend on the packing of the molecules chains and on the order in the solid state as well as on the density of impurities and structural defects.

The purposes of the present paper are as follows: (1) to gain more insights into how the FD molecular layer could promote the formation of the metal oxide at the interface between molecular film and top electrode where the electrical switching is supposed to occur; (2) to analyze the different molecular packing and the band structures of the FD molecular crystals in order to gain information on the mobility in the crystal by comparing the bandwidths of the bands related to the charge transport.

The molecules under examination are fluorescein (FL) in quinone form, FL in lactone form, erythrosine B (ERY), and rose bengal (RB). The molecular structures are sketched in Fig. 1. The molecular crystals considered are FL in salt form, FL in lactone form and ERY.

We calculate the electronic properties of the single molecules within the time-dependent density functional theory (TD-DFT) approach in order to understand the chemical processes that could be implicated in the formation of a metal oxide layer at the top electrode. The TD-DFT has been demonstrated to be successful for modeling dye spectral properties and it can yield results with high accuracy at relatively low computational cost in

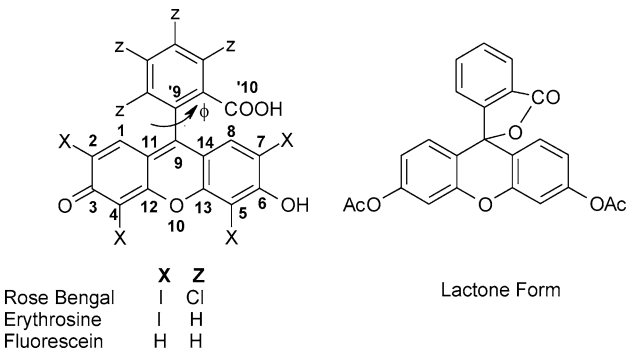

	X	Z
Rose Bengal	I	Cl
Erythrosine	I	H
Fluorescein	H	H

Fig. 1 Molecular structures of the investigated fluorescein dye molecules. The lactone form of the fluorescein is also shown

comparison with highly accurate methods such as multireference configuration interaction (MRC) or complete active space with second-order perturbation theory (CASPT2), which are applicable only to small molecules up to 20 atoms [18, 19]. Moreover, Barone et al. [20] have developed a theoretical multilevel approach for studying the photophysical properties of organic dyes in solution. In particular, they have used accurate force field parameters to simulate MD trajectories. Fluorescence has been calculated at the TD-DFT level on configurations sampled from MD trajectories in order to include time-dependent solvent effects in the computed emission spectrum; this multilevel approach yielded good agreement with respect to experiments. In our case, the electrical bistability has been observed in spin cast films of FDs in which could be relevant the solid state description of electronic properties of molecules.

For the modeling of the electronic properties of the organic crystals, we use the density functional theory (DFT). Although DFT approximation cannot account for van der Waals forces, which are responsible for the cohesion of the molecular solids, this theory provides reliable predictions in covalent and metallic systems. In particular, the use of experimental crystal geometry can guarantee an accurate electronic description. Therefore, we calculated the electronic structure of some fluorescein forms at the GGA level, importing the geometrical structures from crystallographic experiments [21–23] without performing DFT optimization of the geometries.

1.1 Computational details

The crystal DFT calculations in the following section were carried out with the CASTEP code [24] within the generalized gradient approximation (GGA) and with the expression for the exchange and correlation energy introduced by Perdew, Burke, and Ernzerhof (PBE) [25]. The ultrasoft pseudopotentials [26] for atoms and waves up to an energy cutoff of 340 eV were used. A $2 \times 2 \times 3$ Monkhorst and Pack mesh of k-points has been used to sample the Brillouin zone.

The single molecule calculations were performed using Gaussian03 program package [27]. The geometrical parameters of the molecules have been fully optimized at the PBE0 [28] and PBE levels using the LANL2DZ pseudopotentials [29] and corresponding basis set for Cl and I atoms, and 6–31G(d) basis set for all the other atoms. A larger basis set has been used for TDDFT computations, taking the 6–31 + G(d,p) basis set for the lighter atoms. The PBE0 has shown to overcome many of the problems encountered with standard functional, providing accurate excitation energies.

2 Results and discussion

2.1 Crystals

The symmetry system of the unit cell of the FL salt is monoclinic and the edges are a = 13.64 Å, b = 12.60 Å, c = 13.79 Å. The crystallographic angles are $\alpha = 90.000$, $\beta = 97.875$, and $\gamma = 90.000$. There are four molecules per unit cell. The symmetry of the FL in lactone form is triclinic, and the edges of the unit cell are a = 11.04 Å, b = 11.73 Å, and c = 7.37 Å. The crystallographic angles are $\alpha = 95.759$, $\beta = 97.429$, and $\gamma = 94.830$. There are two molecules per unit cell. For simplicity, Na ions were removed from the crystal structure of the salt and the molecules were hydrogenated to restore the neutrality of the cell, thus ionic bands could be ignored. Images of the unit cells of the FL crystals are reported in Fig. 2.

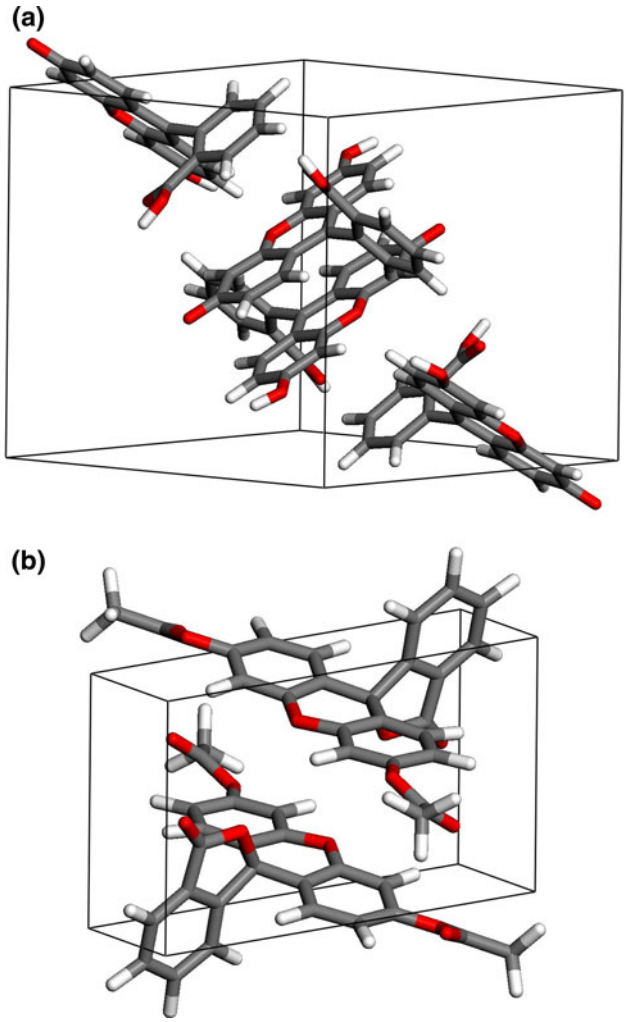

Fig. 2 Unit cell of (**a**) the fluorescein in salt form (from reference 22) and **b** the fluorescein in lactone form (from reference 21) molecular crystals. In the salt, sodium ions have been removed and the molecules hydrogenated (see text for more details)

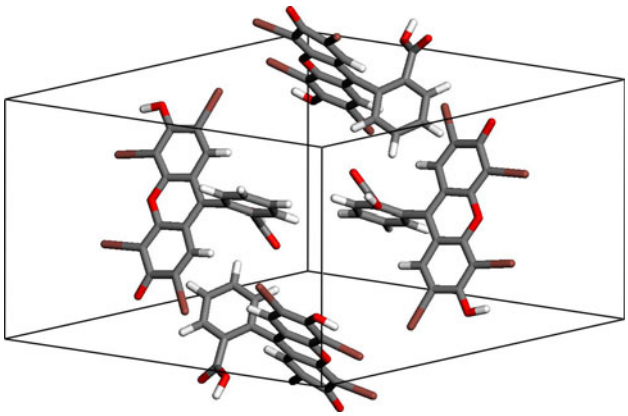

Fig. 3 Unit cell of the erythrosine B molecular crystal (from reference 23). Ethanol and ions have been removed and the molecules hydrogenated (see text for more details)

The symmetry system of the unit cell of the ERY B is monoclinic and the edges are a = 16.13 Å, b = 12.94 Å, and c = 16.37 Å (Fig. 3). The crystallographic angles are $\alpha = 90.000$, $\beta = 134.737$, and $\gamma = 90.000$ with four molecules per unit cell. Ethanol and ions were removed from the crystal structure, while the molecules were hydrogenated to guarantee the electroneutrality.

The three single crystals showed a very different arrangement of molecules; in the sodium salt form of FL, an irregular arrangement was observed along (010) crystallographic axis. In particular, a pair aggregation form was found, in which two xanthene rings are alternated with two phenyl rings. On the contrary, in the lactone form, aggregation structures formed by the xanthene rings in a coplanar organization and in co-facial arrangements are responsible for a regular π–π stacking. This particular structure organization is expected to have a strong impact on the transport properties and to bring significant difference with respect to sodium salt form. Finally, in the ERY B, an irregular arrangement along (010) direction was observed as in FL salt. However, in this case, xanthene and phenyl rings were alternated with partial overlap of π orbitals.

In Figs. 4 and 5, the band structures of the FL crystals in salt and lactone form are plotted and only the energy window between −1.0 and 3.5 eV near the top of the valence band, where the zero of the energy is set, is shown. The band structures of the crystals exhibited small dispersions, which reflected the weak chemical intermolecular interactions. The bandwidth of the HOMO (LUMO)-derived bands were 0.01 (0.04) eV for the salt and 0.03 (0.12) eV for the lactone form. The band gap was $E_g = 1.8$ eV in salt form and $E_g = 3.1$ eV in lactone form. It is well known that GGA functionals underestimate bandgap; nonetheless, we can compare calculated energies for different crystals. In the salt, there are four molecules, and thus each of the HOMO and LUMO bands are formed by 4 bands, with twofold degeneration removed only along the Z–G, G–Y, and B–D paths of the Brillouin zone as plotted in the inset of Fig. 4, where the details of the HOMO and LUMO bands are shown. In the lactone form with two molecules per unit cell, two HOMO- and two LUMO-derived bands are present that are non-degenerate due to the symmetry of the unit cell.

It is interesting to investigate the crystal arrangement and band structure of the ERY crystal (Fig. 6), which is characterized by a molecular symmetry different from that of FL salt. There are four molecules in the unit cell and four HOMO (LUMO)-derived bands with bandwidth

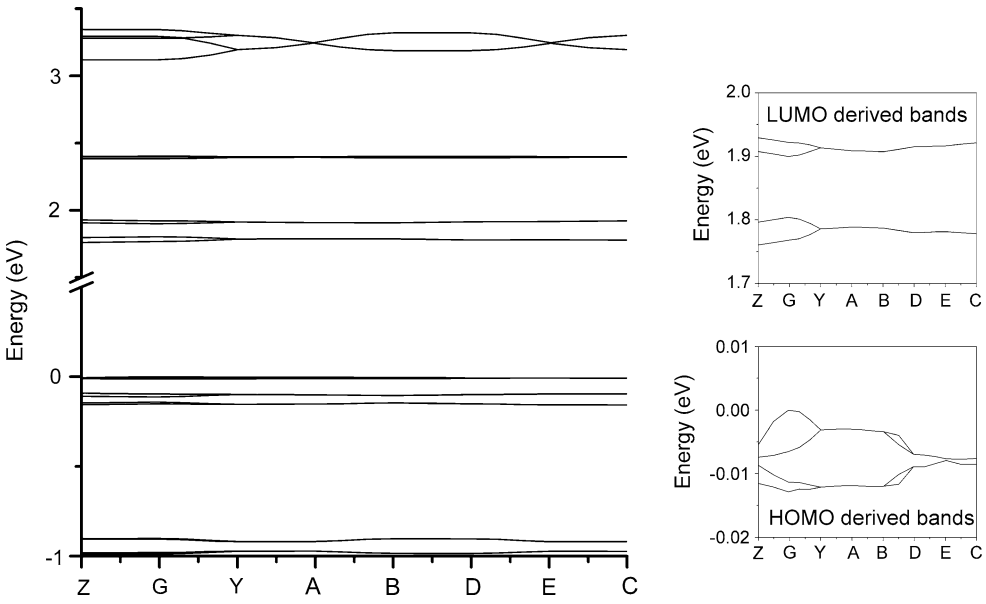

Fig. 4 Band structure of the fluorescein crystal in salt form. In the insets particulars of the HOMO- and LUMO-derived bands are depicted

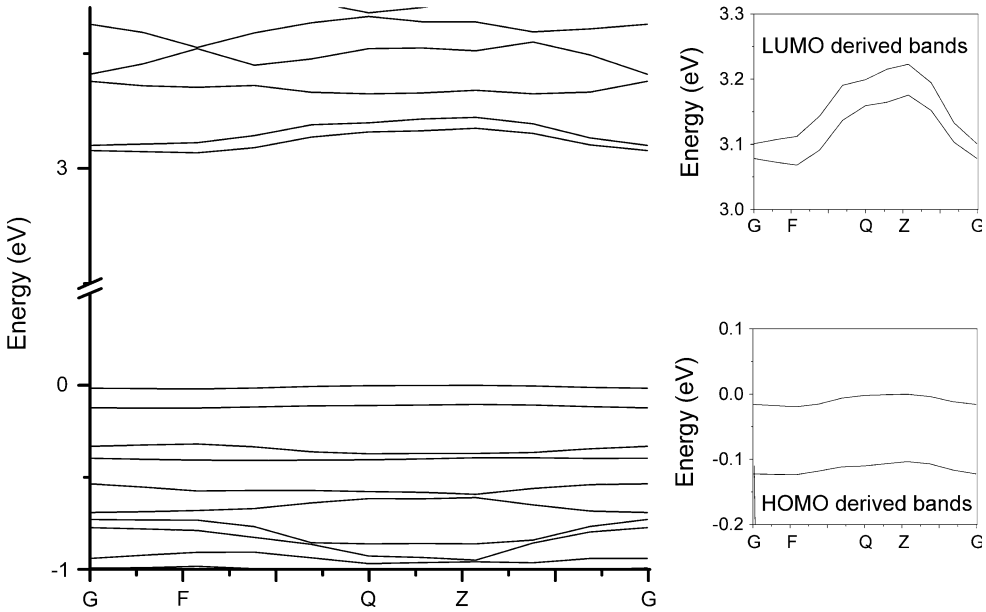

Fig. 5 Band structure of the fluorescein crystal in lactone form. In the insets particulars of the HOMO- and LUMO-derived bands are depicted

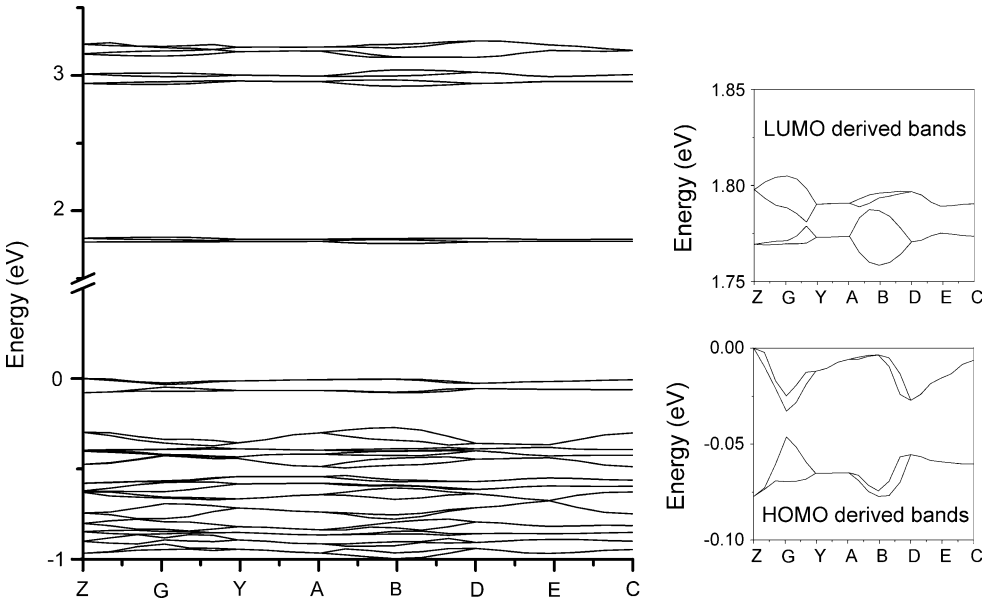

Fig. 6 Band structure of the erythrosine B crystal. In the insets particulars of the HOMO- and LUMO-derived bands are depicted

0.02 (0.03) eV, while the bandgap is $E_g = 1.8$ eV. Therefore, near the energy gap, the band structure is similar to that of the FL salt, but in this case, we have twofold degeneration along Y–A, D–E, and E–C Brillouin zone paths.

We have also calculated the optical absorptions of crystals and single molecules in periodic cells based on the dielectric function expressed in terms of the matrix elements for electronic interband transitions [30]. The DFT single molecule results were obtained by placing a molecule in a large periodic cell in such a way that intermolecular interactions were negligible. We have introduced a 0.5 eV scissor operator [31] to reproduce the absorption spectra of FL and ERY [32]. The results are reported in Table 2.

The simple morphological investigation of the crystal structures can give some insights into the transport properties of the crystals. Indeed, the FL in lactone form stacks in the crystal keeping the molecular planes parallel and allowing a coherent overlap of the π-orbitals. This is not the case for salt and ERY B, where molecular planes change direction in the same unit cell. Therefore, the lactone form should demonstrate improved mobility because of the better molecular order. Also, the band structures gave information on the transport properties of the crystals. It was shown that the bandwidth of the lactone form is

Table 1 Main geometrical parameter (Å and degrees)

	Acid fluorescein			Lactone form			Erythrosine			Rose bengal	
	Exp[a]	Vacuum		Exp[b]	Vacuum		Exp[c]	Vacuum		Vacuum	
		PBE0	PBE		PBE0	PBE		PBE0	PBE	PBE0	PBE
C9–C′9	1.499	1.496	1.495	1.501	1.522	1.520	1.469	1.501	1.494	1.501	1.494
C9–O′10				1.511	1.477	1.498					
$C_{13}O_{10}C_{12}$	120.6	121.4	120.8	120.9	119.2	118.5	121.8	121.5	121.0	121.8	121.2
$C_{14}C_9C_{11}$	119.2	119.6	119.4	117.5	111.3	111.4	119.5	119.7	119.4	120.3	119.9
ϕ	79.21	93.68	105.4				80.95	93.3	96.4	89.88	99.9

The values have been computed at the PBE0 and PBE levels

[a] Ref [22], [b]ref [21], [c]ref [23]

larger than that of the salt, due to better intermolecular interactions. In fact, a large dispersion of the bands is related to a good electronic coupling of the molecules forming the crystal that enhances the electronic mobility within the structure. Very flat bands are a sign of poor interactions, and this was the feature found for FL salt and ERY B, so that the mobility offered by these materials should be low. This can be at the base of the low OFF current reported in the molecular films, in particular in those with halogens. The lack of the crystal structure for RB hindered the investigation of the molecular arrangement and band structure of RB crystal. However, it is expected that this crystal is similar to the ERY B crystal.

2.2 Single molecules

The investigation on single molecules was carried out in order to find the processes that were able to promote the formation of metal oxide layer. It is worth noting that oxide at the interface between organic layer and aluminum electrode can be electrically bistable and it probably causes the resistive switching mechanism d).

The main geometrical parameters at PBE0 and PBE levels of the molecular systems have been collected in Table 1 together with the available X-ray data [21–23]. The atom labeling of FL is reported in Fig. 1. The same labeling was applied to all the molecules of the family. There is an overall satisfactory agreement between the theoretical and the available experimental data. As a general remark, we can state that the systems have similar geometrical rearrangements. It is noteworthy to underline that the torsion angles at PBE0 level are closer to experimental data than corresponding values at PBE level. This is induced by the particular tendency of the PBE approach, compared to that of PBE0, to stabilize conjugated systems.

FDs are photosensitizers capable of adsorbing light in the visible spectrum and using that energy to excite oxygen to its singlet state [33]. Excitation is generally obtained through a one-photon transition between the singlet ground state S_0 and a singlet excited state S_n of the FD. Then, the S_n state relaxes to the lowest excited singlet state S_1. The triplet state T_1 of the FD is generated by intersystem crossing. The lifetime of the T_1 state is longer than that of the S_1 state, so that it can react in one of the following way: (I) free radicals are produced by electron transfer between the excited FD and the molecular substrate. The free radicals can react with oxygen to form active oxygen species, such as singlet oxygen and the superoxide radical anion O_2^{*-}; (II) the excited FD collides with triplet oxygen generating singlet oxygen via an energy transfer process. Both processes can promote the formation of oxide at the heterointerface with metal electrodes.

The energy gap between the singlet ground state S_0 and the lowest triplet state T_1 has been analyzed by carrying out unrestricted PBE0 calculations both at the corresponding S_0 geometries. The calculated energy gaps with respect to the ground electronic state are reported in Fig. 7.

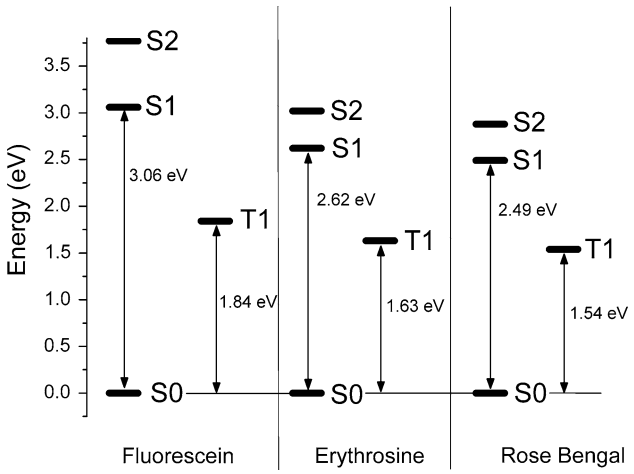

Fig. 7 Excited energy level for singlet and triplet state of fluorescein, erythrosine, and rose bengal

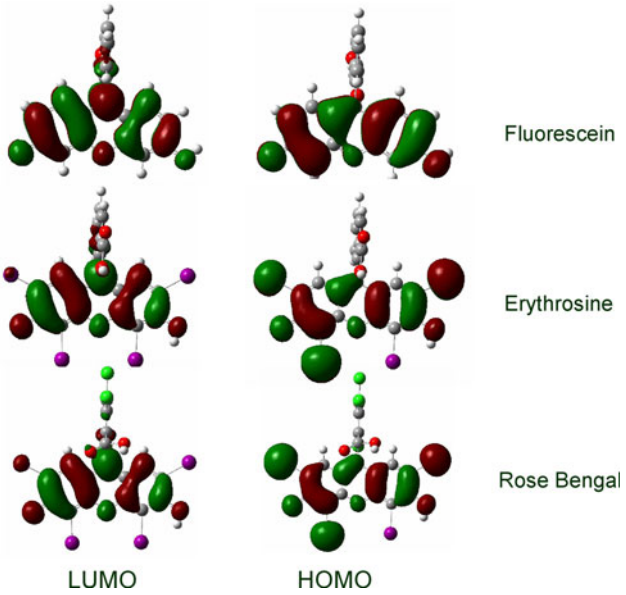

Fig. 8 LUMO and HOMO molecular orbitals of the investigated molecules

In all of the considered systems, the triplet state corresponds to an excitation from the HOMO to the LUMO. In going from the FL to the RB, the S_0/T_1 vertical gap decreases from 1.84 to 1.54 eV. This behavior can be rationalized in terms of the HOMO shape depicted in Fig. 8; in the ERY and RB with heavy halogen mass; this orbital has a significant antibonding C–I. The antibonding character decreases upon excitation of one electron, as it can be deduced from LUMO shapes and then the stability of the molecule increases, decreasing T_1 energy. It can be said that halogens increase the polarizability of the molecule, playing a key role in the systematic decrease in energy gap going from FL to RB, by increasing the atomic weight of the substituent halogens.

The UV spectra have been evaluated using TD-DFT approach, and the results are collected in Table 2.

For the absorption peak calculated with the plane wave basis set, the scissor operator was applied to correct the error of the band gap intrinsic in the GGA-PBE calculation within DFT. In the PBE0 level of calculation within TD-DFT, although no scissor operator was introduced, a quite strong discrepancy between experimental and theoretical values was found in the case of FL. Nevertheless, it is also clear that, as discussed by Neckers [32], the formation of aggregates modified the absorption spectrum, decreasing the quantum yield of singlet oxygen. The lactone form showed a band at high energy due to broken of xantene ring conjugation. The inter-ring cyclization of the lactone changed the hybridization on C9 from sp^2 to sp^3 and shifted the absorption band to low wavelength.

The calculated energy difference between triplet T_1 and the lowest excited singlet state S_1 is reported in Table 3. It is well known that intersystem crossing from S_1/T_1 can be evaluated by Fermi's Golden Rule taking into account the vibronic coupling between the two states. Indeed, the energy gap S_1/T_1 can be considered like a rough evaluation of the quantum yield of the triplet state. Low S_1/T_1 gaps correspond to high triplet yield. Preliminary calculations on the FL in lactone form have shown that the triplet state had a very high energy; therefore, the triplet yield was not enough appreciable to include this molecule in the present discussion.

Among the molecules considered, the RB is the molecule with the strongest oxidation properties in its triplet state. In fact, as evidenced before, the triplet quantum yield was very high and the corresponding singlet oxygen yield was $\phi_\Delta = 0.76$, with intense absorption bands in the green area of the visible spectrum [34]. Therefore, the reduction in the molecule and the consequent formation of oxide layer are highly probable.

The electron affinities (EA) were evaluated as the energy released when an electron was added to a neutral molecule and computed as the energy difference between the neutral form and the anion: $EA = E(M) - E(M^-)$.

The ionization potential (IP) was evaluated as the amount of energy required to remove an electron from a molecule and computed as the energy difference between the cation and the neutral molecule: $IP = E(M^+) - E(M)$. The EA and IP shown in the Fig. 9 have been evaluated taking into account the zero-point energy corrections.

Table 2 Computed TDDFT vertical excitation energies in nm units at PBE0 level for the lowest singlet state

	Acid fluorescein			Lactone form		Erythrosine			Bengal rose	
	TDDFT	DFT	Exp	TDDFT	DFT	TDDFT	DFT	Exp	TDDFT	Exp
S0-S1	404	478 (507)	490	231	253 (260)	472	531 (554)	526	497	549
S0-S2	389					410			430	
S0-S3	328					334			345	

The bands are evaluated using 6–31 + G** basis set at the LANL2DZ geometries. DFT optical absorption peaks in nm units for electronic interband transitions are also reported for crystals; in parenthesis are shown the values for isolated molecules. Experimental data are from Ref. [32]

Table 3 Computed energy gap (eV) between S1 and T1 states

	Energy gap (eV) S1-T1
Fluorescein	1.22
Erythrosine	0.99
Rose bengal	0.95

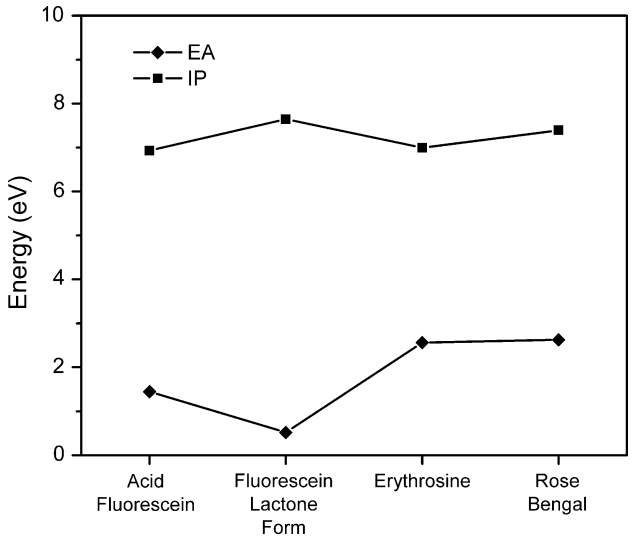

Fig. 9 Electronic affinities and ionization potentials of the molecules

Although the oxidation and reduction potentials were evaluated in solution, a systematic investigation of IP and EA provided an idea about the redox behavior of our systems. A systematic regular behavior can be observed for all the systems with the exception of FL in lactone form. In particular, an increase of the polarizability and of the number of halogen atoms enhances the EA and IP. The high electronic affinity observed for RB supported the hypothesis that the molecule show high tendency to reduce itself oxidizing the electrode.

3 Conclusions

FL in lactone form crystal stacks regularly keeping parallel planes and allowing a coherent overlap of the π-orbitals. Instead, the crystals of the FL salt and ERY B revealed a structure with poor order and weak intermolecular interactions. The irregular spatial arrangement was reflected in the band structures with small bandwidths. Very flat bands indicated poor intermolecular interactions and low charge mobility as well as high resistivity. However, it was found that ERY B and FL salt have similar bandwidths, so that FDs including xanthene rings with halogen substituent atoms have resistivity comparable to that of FL salt without halogen atoms. Therefore, the improved ON/OFF ratio of FDs with halogen substituent atoms would be explained in terms of hetero-interface effects rather than in terms of the internal arrangement of the molecules in the crystal.

The RB showed high quantum yield of the triplet state and, as a result, RB has very strong oxidation properties. Indeed, triplet state could react either by electron transfer producing free radicals that interacted with oxygen to form active oxygen species or via energy transfer process that generates singlet oxygen. On the other hand, the high electronic affinity of RB confirmed the elevated tendency to reduce itself. Those are oxidation mechanisms able to support the formation of electrically bistable thin oxide layer at the organic layer/electrode interface. The ON/OFF ratio depends on the nature of the oxide and layer thickness. Lactone form of FL was characterized by low triplet yield that made films based on this molecule disadvantaged in the formation of oxide layers.

It was found that RB is the molecule more prone to promote the formation of an electrically bistable aluminum oxide layer at the electrode. Further calculations are required to include vibronic contributions, which are essentials to achieve a full picture of the photosensitization mechanisms.

Acknowledgments This study was supported by TRIPODE project DM 20160 of the MIUR, Italy.

References

1. Bandyopadhyay A, Pal AJ (2003) J Phys Chem B 107:2531
2. Bandyopadhyay A, Pal AJ (2004) Appl Phys Lett 84:999
3. Bandyopadhyay A, Pal AJ (2003) Adv Mater 15:1949
4. Bandyopadhyay A, Pal AJ (2005) J Phys Chem B 109:6084
5. Jakobsson FLE, Crispin X, Cölle M, Büchel M, de Leeuw DM, Berggren M (2007) Org Electron 8:559
6. Kärthauser S, Lüssem B, Weides M (2006) J Appl Phys 100: 94504
7. Fazzi D, Castiglioni C, Negri F (2010) Phys Chem Chem Phys 12:1600
8. Schmidt PE, Davila C, Esqueda P, Callarotti R (1975) J Solid State Chem 12:293
9. Ansari AA, Qadeer A (1985) J Phys D 18:911
10. Shirodkar VS, Chourey AG (1988) J Mater Sci Lett 7:1235
11. Gloos K, Koppinen PJ, Pekola JP (2003) J Phys Condens Matter 15:1733
12. Seo S, Lee MJ, Seo DH, Jeoung EJ, Suh DS, Joung YS, Yoo IK, Hwang IR, Kim SH, Byun IS, Kim JS, Choi JS, Park BH (2004) Appl Phys Lett 85:5655
13. Cölle M, Büchel M, de Leeuw DM (2006) Org Electron 7:305
14. Yang JJ, Pickett MD, Li X, Ohlberg DAA, Stewart DR, Williams RS (2008) Nat Nanotechnol 3:429
15. Yoshida TK, Noshiro H, Sugiyama Y (2007) Appl Phys Lett 91:223510
16. Yang MK, Park JW, Ko TK, Lee JK (2009) Appl Phys Lett 95: 042105
17. Sun B, Liu L, Xu N, Gao B, Wang Y, Han D, Liu X, Han R, Kang J (2009) Jpn J Appl Phys 48:04C061

18. Jacquemine D, Perpete EA, Ciofini I, Adamo C (2009) Acc Chem Res 42:326
19. Drew A, Head-Gordon M (2005) Chem Rev 105:4009
20. Barone V, Bloino J, Monti S, Pedone A, Prampolini G (2011) Phys Chem Chem Phys 13:2160
21. Knudsen KD, Pattison P, Fitch AN, Cernik RJ (1998) Angew Chem Int Ed 37:2340
22. Yamaguchi K, Tamura Z, Maeda M (1997) Acta Cryst C 53:284
23. Cody V (1987) Acta Cryst C4(3):705
24. Clark SJ, Segall MD, Pickard CJ, Hasnip PJ, Probert MJ, Refson K, Payne MC (2005) Z Kristallogr 220:567
25. Perdew JP, Burke K, Ernzerhof M (1996) Phys Rev Lett 77:3865
26. Vanderbilt D (1990) Phys Rev B 41:7892
27. Gaussian 03 Revision C.02 (2004) Frisch MJ, Trucks GW, Schlegel HB, Scuseria GE, Robb MA, Cheeseman JR, Montgomery Jr. JA, Vreven T, Kudin KN, Burant JC, Millam JM, Iyengar SS, Tomasi J, Barone V, Mennucci B, Cossi M, Scalmani G, Rega N, Petersson GA, Nakatsuji H, Hada M, Ehara M, Toyota K, Fukuda R, Hasegawa J, Ishida M, Nakajima T, Honda Y, Kitao O, Nakai H, Klene M, Li X, Knox JE, Hratchian HP, Cross JB, Bakken V, Adamo C, Jaramillo J, Gomperts R, Stratmann RE, Yazyev O, Austin AJ, Cammi R, Pomelli C, Ochterski JW, Ayala PY, Morokuma K, Voth GA, Salvador P, Dannenberg JJ, Zakrzewski VG, Dapprich S, Daniels AD, Strain MC, Farkas O, Malick DK, Rabuck AD, Raghavachari K, Foresman JB, Ortiz JV, Cui Q, Baboul AG, Clifford S, Cioslowski J, Stefanov BB, Liu G, Liashenko A, Piskorz P, Komaromi I, Martin RL, Fox DJ, Keith T, Al-Laham MA, Peng CY, Nanayakkara A, Challacombe M, Gill PMW, Johnson B, Chen W, Wong MW, Gonzalez C, Pople JA, Gaussian Inc, Wallingford CT
28. Adamo C, Barone V (1999) J Chem Phys 110:6158
29. Hay PJ, Wadt WR (1985) J Chem Phys 82:284
30. Read AJ, Needs RJ (1991) Phys Rev B 44:13071
31. Godby RW (1992) Top Appl Phys 69:88
32. Neckers DC (1989) J Photochem Photobiol A Chem 47:1
33. DeRosa MC, Crutchley RJ (2002) Coord Chem Rev 233–234:351
34. Redmond RW, Gamlin JN (1999) Photochem Photobiol 70:391